Digging Trajectory Optimization for Cable Shovel Robotic Excavation Based on a Multi-Objective Genetic Algorithm

Qiushi Bi [1] [ID], Guoqiang Wang [1], Yongpeng Wang [2,3], Zongwei Yao [1,4,*] [ID] and Robert Hall [5,*]

[1] School of Mechanical and Aerospace Engineering, Jilin University, Changchun 130025, China; bqs@jlu.edu.cn (Q.B.); wgq@jlu.edu.cn (G.W.)
[2] Taiyuan Heavy Industry Co., LTD., Taiyuan 030024, China; wyp1989318@163.com
[3] State Key Laboratory of Mining Equipment and Intelligent Manufacturing, Taiyuan 030024, China
[4] Key Laboratory of CNC Equipment Reliability, Ministry of Education, Changchun 130025, China
[5] School of Mining and Petroleum Engineering, University of Alberta, Edmonton, AB T6G 2H5, Canada
[*] Correspondence: yzw@jlu.edu.cn (Z.Y.); rhall1@ualberta.ca (R.H.)

Abstract: As one of the most essential earth-moving equipment, cable shovels significantly influence the efficiency and economy in the open-pit mining industry. The optimal digging trajectory planning for each cycle is the base for achieving effective and energy-saving operation, especially for robotic excavation, in which case, the digging trajectory can be precisely tracked. In this paper, to serve the vision of cable shovel automation, a two-phase multi-objective genetic algorithm was established for optimal digging trajectory planning. To be more specific, the optimization took digging time and energy consumption per payload as objects with the constraints of the limitations of the driving system and geometrical conditions. The WK-55-type cable shovel was applied for the validation of the effectiveness of the multi-objective optimization method for digging trajectories. The digging performance of the WK-55 cable shovel was tested in the Anjialing mining site to establish the constraints. Besides, the digging parameters of the material were selected based on the tested data to make the optimization in line with the condition of the real digging operations. The optimization results for different digging conditions indicate that the digging time decreased from an average of 20 s to 10 s after the first phase optimization, and the energy consumption per payload reduced by 13.28% after the second phase optimization, which validated the effectiveness and adaptivity of the optimization algorithm established in this paper.

Keywords: digging trajectory; cable shovel; robotic excavation; multi-objective genetic algorithm

1. Introduction

A cable shovel is one of the key equipment in the open-pit mining industry traditionally operated by trained operators [1]. Abundant research results indicate that human factors have become a main factor inducing maintenance cost and reliability risk [2,3]. Current shovels with larger bucket capacity bring the benefit of lower digging cost, but higher operational difficulty, which makes the concept of robotic excavation a practical option for effective and steady digging processes.

Rational planning of digging trajectory is the base for robotic excavation. Awuah-Offei K. et al. optimized the hoist and crowd speed of a P&H 2100b cable shovel based on the Balovnev model with the objective of minimizing the unit payload energy consumption [4]. Dunbabin M. et al. designed an operation assistant system for cable shovels, which can help the driver plan the digging trajectory and predict the bucket fullness [5]. Wei B. et al. came up with a three degree of freedom (DOF) working mechanism of a cable shovel with an optimal design of the handle structure with the goal of

minimizing the unit payload energy consumption [6]. Wang X. et al. established a digging resistant force model, based on which the digging trajectory of a cable shovel was optimized with a result described by the curves of hoist and crowd velocities [7]. The unit payload energy consumption is commonly taken as the object in digging trajectory optimization. However, the digging efficiency is also a critical factor influencing cable shovel operations, especially for shovels with large bucket capacity. Hence, a multi-objective optimization algorithm should be applied for optimal digging trajectory planning.

Different multi-objective optimization algorithms have been widely used in the design of earth-moving machinery. Xu G. et al. applied the improved multi-objective evolutionary algorithm (MOEA) for TriPower shovel attachment working performance optimization [8]. Jang G. et al. applied the genetic algorithm (GA) on trajectory optimization of the hydraulic excavator for the optimization of energy consumption and the total length of the dig trajectory [9]. Yu X. et al. optimized the design of the bucket of a hydraulic excavator by solving a multi-objective problem, achieving a light-weight and high-strength product [10]. Feng H. et al. focused on the task of precise control of the hydraulic excavator using multi-objective genetic algorithm optimization [11]. Li X. et al. improved the digging efficiency of the hydraulic excavator by optimization of the working mechanism based on the algorithm of parallel PSO [12]. Kim J.-W. et al. optimized the working performance of the hydraulic excavator for multiple objects through the hybrid Taguchi random coordinate search algorithm [13]. Barakat N. and Sharma D. provided an optimal design method for the bulldozer blade based on the evolutionary multi-objective optimization algorithm [14]. Masih-Tehrani M. and Ebrahimi-Nejad S. combined the genetic algorithm and integer linear programming technique for multi-objective optimization of the powertrain of the bulldozer [15]. Zhang Z. and He B. developed a multi-objective optimization platform for wheel loader working mechanism design [16]. Cao B-w. et al. applied a genetic algorithm for multi-objective optimization of the stroke difference for wheel loaders [17].

Compared with other earth-moving equipment, the digging performance of the cable shovel is more difficult to predict because of the huge bucket capacity and the complex digging condition. Hence, optimal planning of the digging trajectory appears to be more necessary for each operation cycle of the cable shovel. In this paper, taking digging time and energy consumption per payload as objects, a two-phase multi-objective optimization based on genetic algorithms is applied for planning a practical digging trajectory with an equal value of the soil cutting angle. The research background is introduced in the first part of this paper. The second part explains how the digging trajectory is generated. In the third part, the model of working performance is established, based on which the optimization procedure is accomplished in the fourth part. A cable shovel with a nominal dipper capacity of about 55 m^3 (Type WK-55) is used for validation of the optimization method in the fifth part. Finally, conclusions are summarized in the last part.

2. Digging Trajectory of the Cable Shovel

According to the classic theory for cable shovel performance evaluation, the soil cutting condition should be kept the same during the whole digging process [18]. Therefore, the digging trajectory is traditionally designed as a logarithmic spiral curve, as shown in Figure 1.

The value of the digging angle δ remains the same when the tip of the shovel bucket tracks the logarithmic spiral curve. Based on the geometrical relationship explained in Figure 1a, the value of polar diameter ρ can be expressed as a function of polar angle φ through integral operation:

$$\frac{\mathrm{d}\rho}{\rho \cdot \mathrm{d}\varphi} = \cot\delta, \rho = \rho_0 \cdot e^{\varphi \cot\delta} \tag{1}$$

(**a**) Logarithmic spiral curve (**b**) Trajectory with constant soil cutting angle
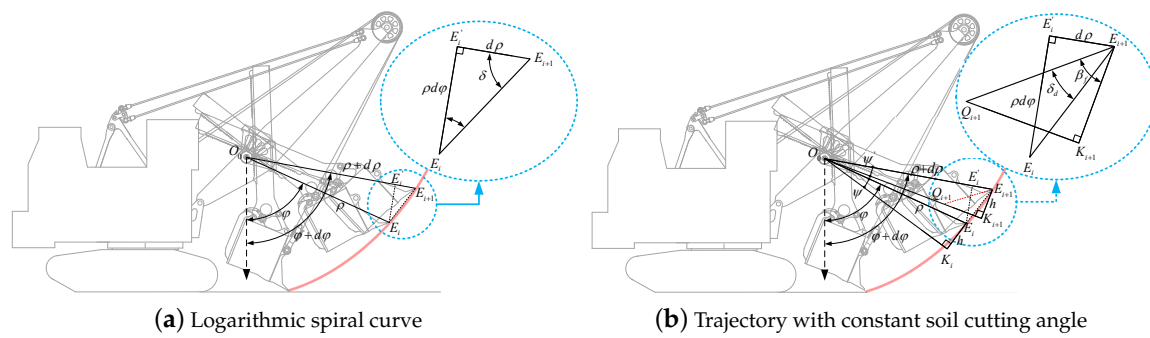
Figure 1. Theoretical digging trajectory for cable shovels.

The symbol ρ_0 indicates the initial value of the polar diameter when the digging process has started. As can be seen from Figure 1a, the digging angle δ cannot fully reflect the impact of the lip front. Therefore, as shown in Figure 1b, based on the logarithmic spiral curve, the curve with a constant value of cutting angle δ_d is developed:

$$\frac{\mathrm{d}\rho}{\rho \cdot \mathrm{d}\varphi} = \cot\left[\left(\frac{\pi}{2} - \psi'\right) - \left(\beta_f - \delta_d\right)\right], \rho = \frac{h}{c} \cdot \left(p_\rho \cdot e^{c \cdot \phi_p} - 1\right) \tag{2}$$

where:

$$\begin{cases} p_\rho = 1 + c \cdot \left(\dfrac{\rho_0}{h} - \dfrac{h}{2 \cdot \rho_0}\right) \\[2mm] \phi_p = \varphi - \arcsin\left(\dfrac{h}{\rho}\right) \\[2mm] c = \tan\left(\beta_f - \delta_d\right) \end{cases} \tag{3}$$

For the convenience of programming, the value of the angle ψ_i in iterative step i can be calculated using the value of the polar diameter in iterative step $i - 1$:

$$\psi_i = \frac{h}{\rho_{i-1}} \tag{4}$$

Combining Equations (2)–(4), the theoretical digging trajectory with a constant digging angle can be established by setting the value of the initial polar diameter ρ_0 and cutting angle δ_d.

Even though the curve with constant soil cutting angle δ_d can theoretically maintain the same digging condition, it is difficult to track this kind of digging trajectory practically. The working device of the cable shovel is a two DOF mechanism as shown in Figure 2. Corresponding to such a theoretical digging trajectory, either the hoist speed or the crowd speed changes from a non-zero value and ends up with another non-zero value. Taking the digging trajectory generated through the parameters shown in Table 1 as an example, the hoist speed curve and crowd speed curve are shown in Figure 3.

Table 1. Digging trajectory parameter: an example.

ρ_0 (m)	δ_d (degree)	φ (degree)	β_f (degree)	Dig Time t_D (s)
9.5	49.3	0–90	51.6	10.281
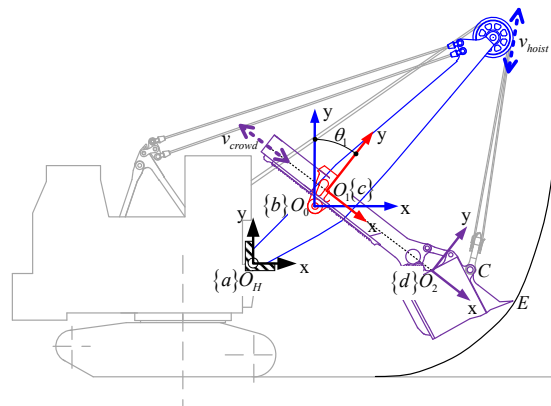
Figure 2. Cable shovel working mechanism.
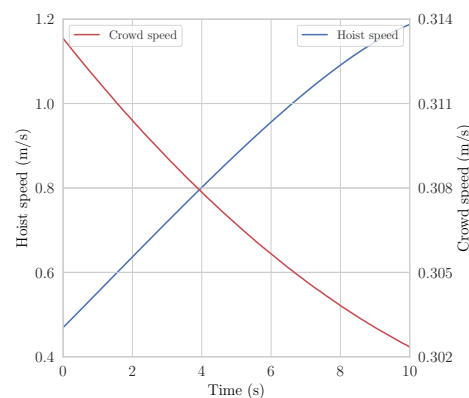
Figure 3. Hoist speed and crowd speed.

It can be clearly seen from Figure 3 that both the speed curves start and end with a non-zero value. However, the working mechanism is commonly locked in a fixed position at the beginning and the ending moment of the digging process, which means the values of the instantaneous speed and acceleration should be zero. Therefore, the contradiction between the digging theory and real operational situation makes it hard to implement the theoretical speed curves. Besides, considering the cable shovel being operated by trained operators, it is difficult for them to control the motors precisely to follow the theoretical speed curves.

Although the advanced control technique applied in a robotic excavation system can accomplish the task precisely tracking the speed curves, it still cannot overcome the contradiction between the theoretically designed speed and the speed that can be operated at the beginning and finishing period of the digging process. Therefore, under the premise of the shovel power capabilities, the main task for digging trajectory optimization for cable shovel robotic excavation can be summarized as two aspects: firstly, taking advantage of the theoretical trajectory with a constant soil cutting angle to acquire optimal working performance; secondly, modifying the corresponding speed curves to to make the digging trajectory practical.

3. Working Performance Modeling

For a certain type of cable shovel, the different speed combinations determine different digging trajectories, reflecting different digging performance such as digging force, digging efficiency, digging power consumption and bucket fullness. The basis for the numerical evaluation of cable shovel working performance is the kinematic analysis of the working mechanism.

3.1. Kinematic Modeling

Establish the Cartesian coordinate system as shown in Figure 2. The polar diameter $\rho(t)$ corresponds to $l_{O_1O_2}(t)$, and the polar angle $\varphi(t)$ transforms into $\theta_1(t)$.

As shown in Figure 2, $v_{crowd} = \dot{l}_{O_1O_2}$, the radius of the saddle block can be symbolized as r_1. Based on the principle shown in Figure 4, the initial distance of l_{C_qC} can be symbolized as $l_{C_qC_0}$, and the angle of η_C can be calculated as $\eta_C = \arctan \frac{l_{C_qC_0} + \dot{l}_{O_1O_2} \times t}{r_1 + H_C} - \left(\frac{\pi}{2} - \theta_1\right)$. Hence, the hoist speed can be calculated through the equations:

$$v_{hoist} = l_{O_0C} \times \dot{\theta}_1 \times \cos \beta_C - \dot{l}_{O_1O_2} \times \cos \varepsilon_C \tag{5}$$

where:

$$\begin{cases} l_{O_0C} = \sqrt{(r_1 + H_C)^2 + \left(l_{C_qC_0} + \dot{l}_{O_1O_2} \times t\right)^2} \\ \beta_C = \arcsin\left(\frac{R_{O_T}}{l_{O_TC}}\right) - \left[\frac{\pi}{2} - \arccos \frac{l_{O_0C}^2 + l_{O_TC}^2 - l_{O_0O_T}^2}{2 \times l_{O_0C} \times l_{O_TC}}\right] \\ l_{O_TC} = \sqrt{l_{O_0C}^2 + l_{O_0O_T}^2 - 2 \times l_{O_0C} \times l_{O_0O_T} \times \cos(\eta_C + \delta)} \\ \varepsilon_C = \arctan\left(\frac{l_{C_qC_0} + \dot{l}_{O_1O_2} \times t}{r_1 + H_C}\right) + \beta_C \end{cases} \tag{6}$$

It is necessary to analyze the speed of the bucket tip for the purpose of confirming the direction of the digging force. Figure 5 shows the principle of the calculation:

$$\begin{cases} v_{Ea} = \sqrt{v_{Ee}^2 + \dot{l}_{O_1O_2}^2 - 2 \times v_{Ee} \times \dot{l}_{O_1O_2} \times \cos \varphi_E} \\ v_{Ea} = \sqrt{(r_1 + H_E)^2 + \left(l_{E_qE_0} + \dot{l}_{O_1O_2} \times t\right)^2} \times \dot{\theta}_1 \\ \gamma_E = \arccos\left(\frac{v_{Ea}^2 + \dot{l}_{O_1O_2}^2 - v_{Ee}^2}{2 \times v_{Ea} \times \dot{l}_{O_1O_2}}\right) \end{cases} \tag{7}$$

where:

$$\varphi_E = \arctan\left(\frac{l_{E_qE_0} + \dot{l}_{O_1O_2} \times t}{r_1 + H_E}\right) \tag{8}$$

The mass of the bucket-handle assembly for a large cable shovel cannot be ignored as it will cause non-negligible inertia force. The principle for the speed analysis is shown in Figure 5:

$$\begin{cases} v_{gax} = \dot{l}_{O_1O_2} \times \cos \theta_1 + l_{O_0G} \times \dot{\theta}_1 \times \cos \eta_G \\ v_{gay} = \dot{l}_{O_1O_2} \times \sin \theta_1 + l_{O_0G} \times \dot{\theta}_1 \times \sin \eta_G \end{cases} \tag{9}$$

where:

$$l_{O_0G} = \sqrt{(r_1 + H_G)^2 + \left(l_{G_qG_0} + \dot{l}_{O_1O_2} \times t\right)^2} \tag{10}$$

Figure 6 explains the composition principle of acceleration:

$$a_{gax} = -a_{gen} \cdot \cos \eta_G + a_{get} \cdot \sin \eta_G + a_{gr} \cdot \cos\left(\frac{\pi}{2} - \varphi_G + \eta_G\right) \pm a_{gc} \cdot \cos(\varphi_G + \eta_G) \tag{11}$$

$$a_{gay} = a_{gen} \cdot \sin \eta_G + a_{get} \cdot \cos \eta_G - a_{gr} \cdot \sin\left(\frac{\pi}{2} - \varphi_G + \eta_G\right) \pm a_{gc} \cdot \sin(\varphi_G + \eta_G) \tag{12}$$

where:

$$a_{gen} = l_{O_0G} \cdot \left(\dot{\theta}_1\right)^2, a_{get} = l_{O_0G} \cdot \ddot{\theta}_1, a_{gr} = \ddot{l}_{O_1O_2}, a_{gc} = 2 \cdot \dot{\theta}_1 \cdot \dot{l}_{O_1O_2} \tag{13}$$

As can be seen in Equations (11) and (12), the Coriolis acceleration a_{gc} determines whether to take the positive sign or the negative sign for calculation.
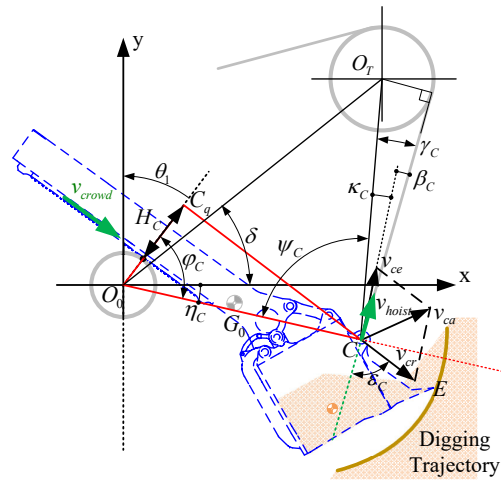
Figure 4. Hoist speed.
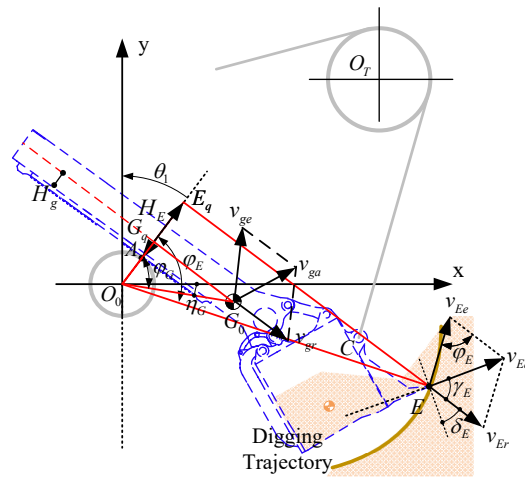
Figure 5. Speed of the bucket tip and handle.
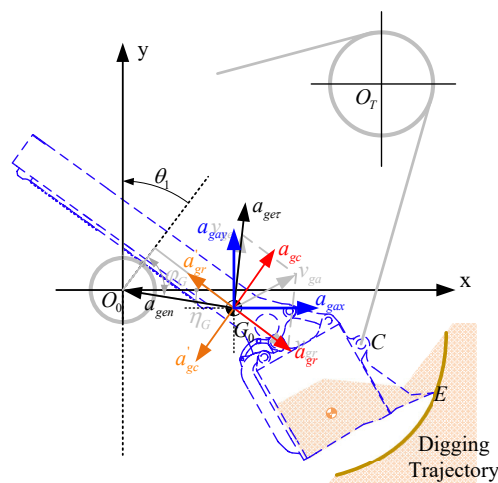
Figure 6. Acceleration of the bucket handle.

3.2. Power Consumption and Bucket Fullness

The forces applied to the bucket-handle assembly during the digging process are shown in Figure 7. The power consumption corresponding to the digging trajectory can be calculated based on the driven speed and applied forces. Figure 8 shows the principle of digging volume evaluation, which can be described as an integration process of the product between digging thickness and bucket width.

The digging forces acting on the tip of the bucket can be simplified as a tangential force and a normal force [18]. Generally, those two forces can be calculated as:

$$\begin{cases} F_{Et}(t) = K \cdot b \cdot c(t) \\ F_{En}(t) = \lambda \cdot F_{Et}(t) \end{cases} \tag{14}$$

Different kinds of material correspond to different digging performance even for the same digging trajectory. Theoretically, the digging resistant force can be simplified as one tangential force and one normal force acting on the bucket tip of the mining shovel when digging the material of sand, loam, gravel or clay. It should be noted that large number of boulders or oversized rocks would lead to significant fluctuation of digging force during the excavation, which makes it difficult to describe the digging process numerically. In Equation (14), the parameter K stands for the unit resistance to excavation whose value depends on the soil type [18], b for the width of the bucket, and $c(t)$ for the current cutting thickness of the soil. The multiplication of $b \cdot c(t)$ represents the area of the current digging cross-section. The parameter of λ in Equation (14) is the ratio between the tangential force and the normal force, whose value depends on the soil type and the service time of the bucket [18].
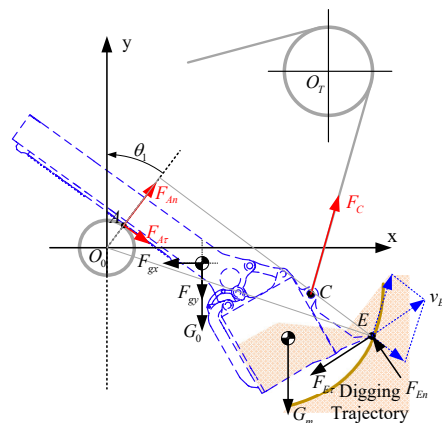
Figure 7. Digging forces' analysis.
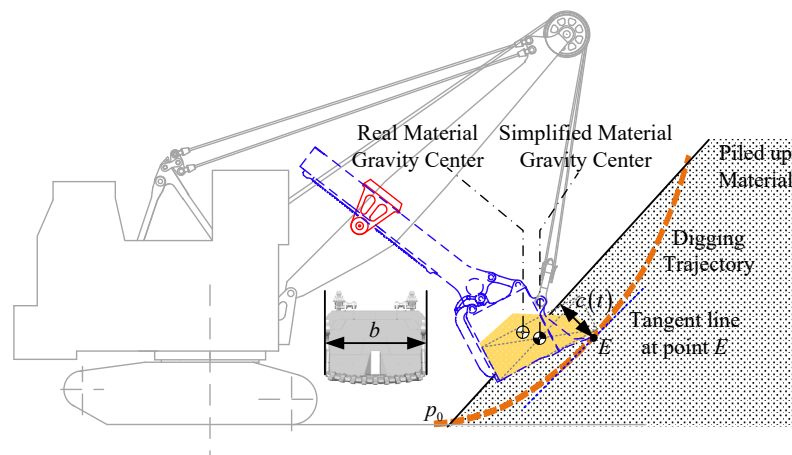
Figure 8. Digging material volume.

Taking advantage of D'Alembert's principle, the crowding force $(F_{crowd} = F_A)$ and hoisting force $(F_{hoist} = F_C)$ can be calculated based on the equilibrium condition shown in Figure 7. Accordingly, the following integral operations can be used for the calculation of energy consumption:

$$E_{hoist} = \int_{t_0}^{t_T} F_{hoist} \times v_{hoist} \, dt \tag{15}$$

$$E_{crowd} = \int_{t_0}^{t_T} F_{crowd} \times v_{crowd} \, dt \tag{16}$$

As shown in Figure 8, the excavated mass and the bucket fullness can be calculated as:

$$M_{dig} = \rho_{soil} \times b \times \int_{t_0}^{t_T} c\,(t) \, dt \tag{17}$$

$$Fullness_{bucket} = \frac{b \times \int_{t_0}^{t_T} c\,(t) \, dt}{V_{bucket}} \tag{18}$$

where the parameter ρ_{soil} stands for the bulk density of the excavated material.

Finally, the unit energy consumption per payload and unit digging time per payload can be calculated through the following equations:

$$E_M = \frac{E_{hoist} + E_{crowd}}{M_{dig}} \tag{19}$$

$$T_M = \frac{t_T - t_0}{M_{dig}} \tag{20}$$

4. Multi-Objective Optimization Procedure

For optimal digging trajectory planning for robotic excavation in each digging cycle, a kind of two-phase multi-objective optimization is applied for the maximum digging efficiency and minimum unit energy consumption. The first phase of optimization can be described as searching the optimal theoretical digging trajectory with a constant soil cutting angle. The second phase, however, is a process making the trajectory practical by optimizing the speed curves of driving systems.

More specifically, for each unique digging condition, the parameters describing the theoretical digging trajectory such as initial polar diameter ρ_0, cutting angle δ_d, and digging time t_d are taken as variables in the first phase of optimization. Accordingly, the working performance and geometrical limitations are taken as constraints. The genetic algorithm is applied for the first phase of multi-objective optimization. Based on the optimized theoretical digging trajectory, four speed control moments are set up: t_1, t_2, t_3, t_4. The time period $0 - t_1$ is an acceleration period, and the speed of both the hoisting and crowding system increase from zero with the value of acceleration rising from zero simultaneously. The time period $t_1 - t_2$ is also an acceleration period with the speed continuously increasing while the value of acceleration diminishes. Either the value of speed or acceleration matches the theoretical trajectory at the moment of t_2. During the time period $t_2 - t_3$, both the speed and acceleration match with that of the theoretical trajectory. The time period $t_3 - t_4$ is a deceleration period, and both the hoist and crowd speed start decreasing with the value of deceleration rising from zero. The last time period $t_4 - t_d$ is also a deceleration period, and either the speed or the deceleration diminishes to zero at the moment t_d. Therefore, the second phase of optimization takes the four speed control moments as variables to make the theoretical digging trajectory practical and further decrease the unit energy consumption. The procedure of the two-phase digging trajectory optimization can be summarized as the flowchart shown in Figure 9.
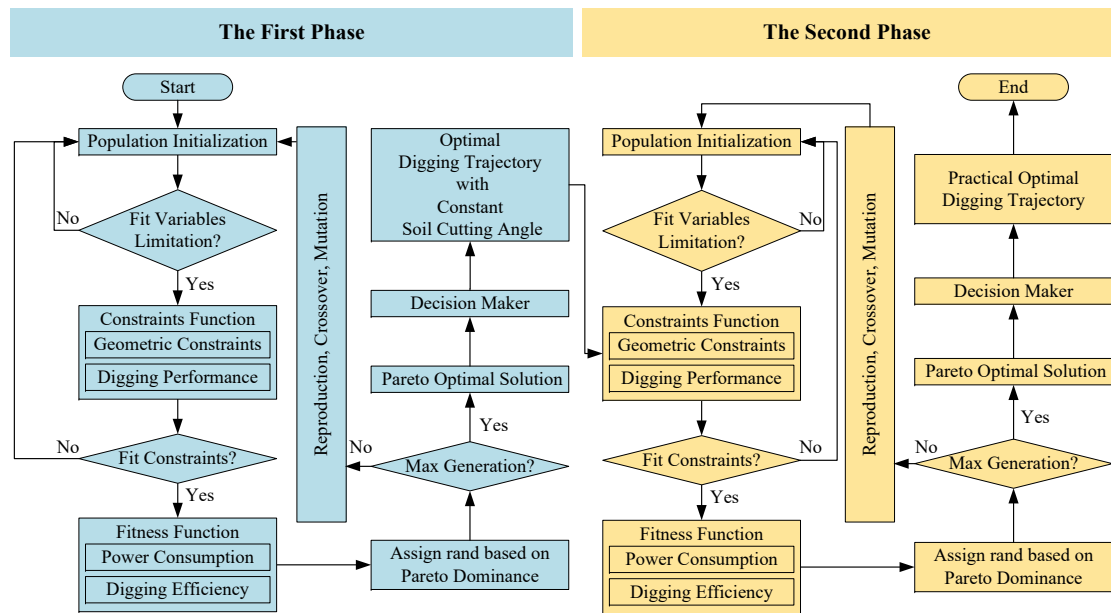
Figure 9. The two-phase multi-objective optimization of the digging trajectory based on the genetic algorithm.

4.1. First Phase Optimization

4.1.1. Variables and the Boundary Constraints

The variables in the first phase optimization are initial polar diameter ρ_0, cutting angle δ_d, and digging time t_d. Generally, the boundary values of the variables are determined by structural and operational limits:

$$X_1 = [\rho_0, \delta_d, t_d] \tag{21}$$

$$\begin{cases} Lower_{X_1} = \left[\rho_{min}, \delta_{dmin}, t_{digmin}\right] \\ Lower_{X_1} = \left[\rho_{max}, \delta_{dmax}, t_{digmax}\right] \end{cases} \tag{22}$$

4.1.2. Fitness Function for Multi-Objective Optimization

In order to make the working performance of unit energy consumption and unit digging time fitness functions applied in the multi-objective genetic algorithm, the parameters of rated hoisting power P_h, rated crowding power P_c, standard digging time t_{ST}, and rated digging mass M_{SAE} are applied for the normalization process:

$$\begin{cases} Fitness_1(X_1) = max\left[\dfrac{(P_h + P_c) \times t_{ST}/M_{SAE}}{E_M(X_1)}\right] \\ Fitness_2(X_1) = max\left[\dfrac{t_{ST}/M_{SAE}}{T_M(X_1)}\right] \end{cases} \tag{23}$$

4.1.3. Constraints

The constraints applied in the first phase of optimization can be summarized as two main kinds: geometrical and performance constraints.

The geometrical constraints can be listed as:

- The position of the bucket should be above the material pile when the digging process finishes:

$$\begin{cases} g_1\left(X_1\right) = y_{slope_{tip}}\left(X_1\right) - y_{bucket_{tip}}\left(X_1\right) < 0 \\ g_2\left(X_1\right) = y_{slope_{bot}}\left(X_1\right) - y_{bucket_{bot}}\left(X_1\right) < 0 \end{cases} \tag{24}$$

In Equation (24), the parameter $y_{slope_{tip}}$ stands for the height of the material piled-up slope corresponding to the bucket tip, while the parameter of $y_{slope_{bot}}$ indicates the slope height corresponding to the bucket bottom. Similarly, the parameter of $y_{bucket_{tip}}$ means the height of the bucket tip itself, while the parameter of $y_{bucket_{bot}}$ stands for the height of the bucket bottom.

- The length of the polar diameter should be within the limitation when the digging process finishes:

$$g_3\left(X_1\right) = \rho_{stop}\left(X_1\right) - \rho_{lim} < 0 \tag{25}$$

In Equation (25), the parameter ρ_{stop} stands for the length of the polar diameter when the digging process finishes, while the parameter ρ_{lim} means the maximum length of the polar diameter.

The performance constraints can be listed as:

- The highest hoist speed during the digging process $v_{hoist_{max}}$ should be smaller than the rated value $v_{hiost_{lim}}$. Similarly, the highest crowd speed $v_{crowd_{max}}$ should not exceed the boundary value of $v_{crowd_{lim}}$ as well.

$$\begin{cases} g_4\left(X_1\right) = v_{hoist_{max}}\left(X_1\right) - v_{hiost_{lim}} < 0 \\ g_5\left(X_1\right) = v_{crowd_{max}}\left(X_1\right) - v_{crowd_{lim}} < 0 \end{cases} \tag{26}$$

- The highest hoist force during the digging process $F_{hoist_{max}}$ should be smaller than the rated value $F_{hiost_{lim}}$. Similarly, the highest crowd force $F_{crowd_{max}}$ should not exceed the boundary value of $F_{crowd_{lim}}$ as well.

$$\begin{cases} g_6\left(X_1\right) = F_{hoist_{max}}\left(X_1\right) - F_{hiost_{lim}} < 0 \\ g_7\left(X_1\right) = F_{crowd_{max}}\left(X_1\right) - F_{crowd_{lim}} < 0 \end{cases} \tag{27}$$

- The highest hoist power during the digging process $P_{hoist_{max}}$ should be smaller than the rated value $P_{hiost_{lim}}$. Similarly, the highest crowd power $P_{crowd_{max}}$ should not exceed the boundary value of $P_{crowd_{lim}}$ as well.

$$\begin{cases} g_8\left(X_1\right) = P_{hoist_{max}}\left(X_1\right) - P_{hiost_{lim}} < 0 \\ g_9\left(X_1\right) = P_{crowd_{max}}\left(X_1\right) - P_{crowd_{lim}} < 0 \end{cases} \tag{28}$$

- An extreme large value of bucket fullness would result in the overload of the power system. In other words, the maximum value of the bucket fullness has already been limited by the constraints of digging power. Hence, the bucket fullness should meet the minimum requirement when the digging process finishes:

$$g_{10}\left(X_1\right) = Fullness_{bucket_{lim}} - Fullness_{bucket}\left(X_1\right) < 0 \tag{29}$$

4.2. Second Phase Optimization

4.2.1. Variables and the Boundary Constraints

In the second phase of optimization, the variables change into the four speed control moments:

$$X_2 = [t_1, t_2, t_3, t_4] \tag{30}$$

The boundary values of the variables can be described as:

$$\begin{cases} Lower_{X_2} = [t_{1min}, t_{2min}, t_{3min}, t_{4min}] \\ Lower_{X_2} = [t_{1max}, t_{2max}, t_{3min}, t_{4max}] \end{cases} \tag{31}$$

4.2.2. Fitness Function for Multi-Objective Optimization

The fitness functions for the second phase of optimization are similar to the first phase. However, it should be noted that the digging trajectory in the second phase of optimization is calculated through the hoist and crowd speed while directly through the variables in the first phase:

$$\begin{cases} Fitness_1(X_2) = max \left[\dfrac{(P_h + P_c) \times t_{ST}/M_{SAE}}{E_M(X_2)} \right] \\ Fitness_2(X_2) = max \left[\dfrac{t_{ST}/M_{SAE}}{T_M(X_2)} \right] \end{cases} \tag{32}$$

4.2.3. Constraints

The constraints applied in the second phase of optimization can be divided into two groups: the same constraints used in the first phase, which can be described as $g_1(X_2) \sim g_{10}(X_2)$, and the unique constraints for the second phase. For geometrical constraints, the limitation for the initial digging point is added to avoid deep insertion into the material at the beginning of the digging process.

$$g_{1a}(X_2) = y_{0slope}(X_2) - y_{0bucket}(X_2) < 0 \tag{33}$$

In Equation (33), the parameter y_{0slope} stands for the height of the material slope corresponding to the bucket tip, while the parameter $y_{0bucket}$ indicates the height of the bucket tip itself.

For the performance constraints, the unique requirements for the speed curve and acceleration curve are taken into consideration.

- At the moment of t_d, both the speed and acceleration for the driving system equal zero:

$$\begin{cases} g_{2a}(X_2) = v_{hoist_{t_d}}(X_2) = 0 \\ g_{3a}(X_2) = v_{crowd_{t_d}}(X_2) = 0 \\ g_{4a}(X_2) = a_{hoist_{t_d}}(X_2) = 0 \\ g_{5a}(X_2) = a_{crowd_{t_d}}(X_2) = 0 \end{cases} \tag{34}$$

- At the moment of t_1 and t_4, the speed and acceleration for the driving system are continuous:

$$\begin{cases} g_{6a}(X_2) = v_{hoist_{t_i}-B}(X_2) - v_{hoist_{t_i}-A}(X_2) = 0 \\ g_{7a}(X_2) = v_{crowd_{t_i}-B}(X_2) - v_{crowd_{t_i}-A}(X_2) = 0 \\ g_{8a}(X_2) = a_{hoist_{t_i}-B}(X_2) - a_{hoist_{t_i}-A}(X_2) = 0 \\ g_{9a}(X_2) = a_{crowd_{t_i}-B}(X_2) - a_{crowd_{t_i}-A}(X_2) = 0 \\ i = 1, 4 \end{cases} \tag{35}$$

In Equation (35), the subscript $'-B'$ represents the parameter value calculated from the time period t_{i-1} to t_i, while the subscript $'-A'$ for the time period t_i to t_{i+1}.

- At the moment of t_2 and t_3, the speed and acceleration for the driving system are continuous, and the parameters of movements match the theoretical digging trajectory.

$$\begin{cases} g_{10a}\left(X_2\right) = v_{hoist_{t_j}}\left(X_2\right) - v_{hoist_{t_j}-theory}\left(X_2\right) = 0 \\ g_{11a}\left(X_2\right) = v_{crowd_{t_j}}\left(X_2\right) - v_{crowd_{t_j}-theory}\left(X_2\right) = 0 \\ g_{12a}\left(X_2\right) = a_{hoist_{t_j}}\left(X_2\right) - a_{hoist_{t_j}-theory}\left(X_2\right) = 0 \\ g_{13a}\left(X_2\right) = a_{crowd_{t_j}}\left(X_2\right) - a_{crowd_{t_j}-theory}\left(X_2\right) = 0 \\ g_{14a}\left(X_2\right) = \rho_{t_j}\left(X_2\right) - \rho_{t_j-theory}\left(X_2\right) = 0 \\ j = 2,3 \end{cases} \tag{36}$$

- The maximum acceleration should be limited in a certain range according to the driving system.

$$\begin{cases} g_{15a}\left(X_2\right) = a_{hoist_{max}}\left(X_2\right) - a_{hiost_{lim}} < 0 \\ g_{16a}\left(X_2\right) = a_{crowd_{max}}\left(X_2\right) - a_{crowd_{lim}} < 0 \end{cases} \tag{37}$$

4.3. Optimization Method

The multi-objective genetic algorithm (MOGA) was applied in either of the two periods of optimization. The MOGA toolbox provided with the MATLAB (R2019a, MathWorks, Natick, MA, USA) software was used for the calculation. After getting the Pareto solution set, the digging time was taken as an indicator for choosing the optimal result. Based on the optimization results, the digging trajectory was generated with the digging performance numerically evaluated. The optimization method should be taken in various situations to validate the efficiency.

5. Case Study

In order to validate the efficiency of the two-phase optimization method, the cable shovel with the nominal dipper capacity of about 55 m^3 (Type WK-55) was used in this research for optimal digging trajectory planning. It was important to determine the constraint's boundaries before the optimization. Therefore, field tests were performed to get the limitations of the working performance.

5.1. Digging Performance Field Test

Considering the digging efficiency, the experienced operators of cable shovels could make the digging operation faster with a higher value of the bucket fullness, which makes the shovel power fully loaded or overloaded during the digging process. Field tests were performed at the Anjialing open-pit coal mining site (Shanxi Province, China), as shown in Figure 10a. The digging performance corresponding to the digging trajectory was recorded through the DAQ system (data acquisition system).

(**a**) WK-55 field operation in the Anjialing mining site   (**b**) Recorded bucket trajectories
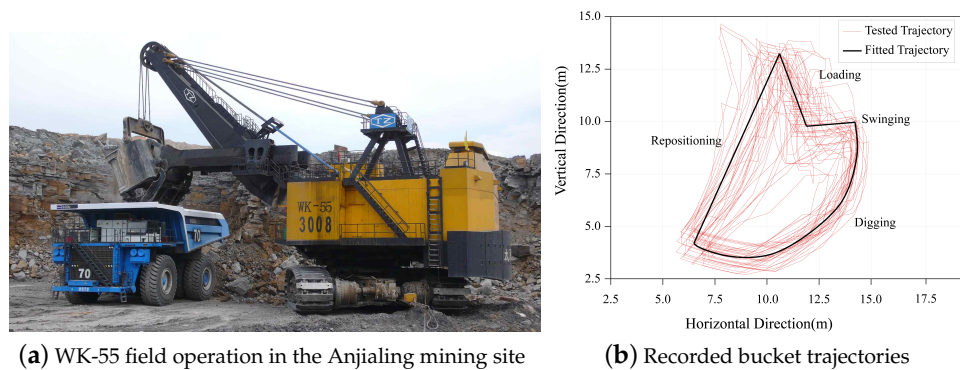
Figure 10. WK-55-type cable shovel field tests.

As can be seen from Figure 10b, the digging trajectories were discrete when the equipment was operated by the operators. The corresponding performance boundaries are listed in Table 2.

Table 2. The tested digging performance boundaries.

No.	Tested Parameters	Unit	Hoist System	Crowd System
1	Maximum torque of a single driven motor	N·m	33,695	9356
2	Maximum force of a single driven motor	kN	1987	1002
3	Maximum speed of a single driven motor	rpm	930	772
4	Maximum power of a single driven motor	kW	1735	754
5	Average time of a digging cycle	s	20	20
6	Minimum time of a digging cycle	s	15	15
7	Maximum mechanism acceleration	m/s^2	0.8	0.5
8	Maximum mechanism velocity	m/s	1.76	0.76

The performance constraints applied for optimization could be established based on the data shown in Table 2 with the value of the overload ratio taken into consideration. Similarly, it was necessary to numerically describe the digging condition to set up the geometrical constraints for the optimization.

5.2. Digging Conditions

The digging pattern for cable shovels could be described as two main steps: Firstly, the equipment stayed at a fixed place for several digging cycles until digging conditions could not meet the operation requirements. Secondly, the cable shovel moved to the next fixed place and repeated the digging process as described in the first step. Hence, the parameters describing the digging condition should be defined in the same coordinate attached to the cable shovel. As shown in Figure 11a, under the circumstances that the profile of the piled-up material was simplified as a straight line, different digging conditions could be described as different combinations of slope angle δ_m and digging distance d_m. Generally, the value of the slope angle ranges from $37°$ to $42°$ for blasted rock. However, for the digging distance, the minimum value should keep the tip of the bucket from not contacting the material slope. The structural parameters of the WK-55-type cable shovel are explained in Figure 11b and listed in Table 3.

(**a**) Relevant position parameters   (**b**) Structural parameters
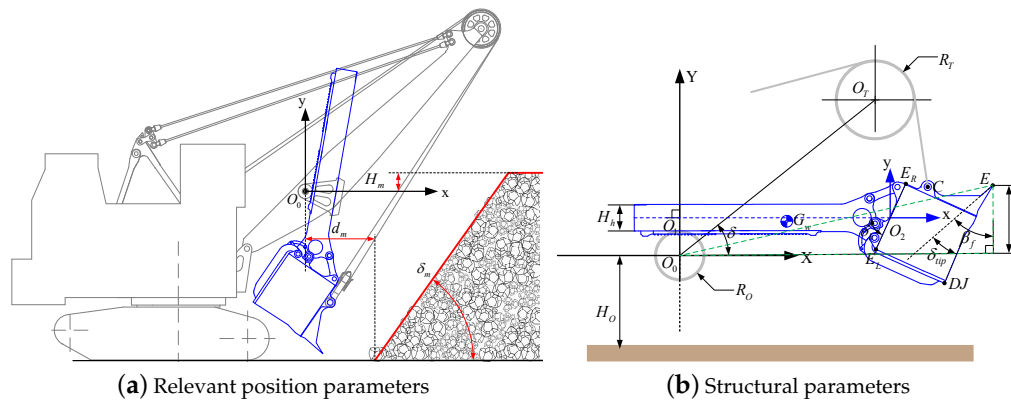
Figure 11. Digging conditions.

Table 3. Structural parameters of the WK-55 cable shovel working device.

H_h (m)	H_o (m)	R_o (m)	R_T (m)	h (m)	β_f (degree)	δ (degree)	δ_h (degree)	δ_{tip} (degree)
1.37	10.14	0.368	1.11	2.35	51.7	44.4	60.9	6.8

Additionally, the material parameters should be chosen carefully to evaluate the digging force and other digging performance rationally. On the basis of the tested data gained from the Anjialing mining site, the parameters indicating digging force are determined with the combination of the measured trajectories to make the optimization process stay in line with the real digging condition. The parameters of the excavated material in the Anjialing mining site, as well as the parameters of the WK-55 shovel bucket are listed in Table 4.

Table 4. Material property and WK-55 bucket parameters.

ρ_{soil} (kg/m^3)	K (kpa)	λ	b (m)	V_{bucket} (m^3)	M_{handle} (kg)	M_{bucket} (kg)
1700	225	0.45	4.86	58	42,514	84,421

5.3. First Phase Optimization

In the first phase optimization, the digging conditions were divided into two main categories according to the different profiles of the piled-up material: the flat surface, which could be described using a slope angle, and the curved surface defined by groups of coordinate values.

5.3.1. Material Piled up with a Flat Surface

As listed in Table 5, five different digging conditions were set up for the first phase digging trajectory optimization.

Table 5. Parameters describing digging conditions.

Digging Condition Number	δ_m (degree)	d_m (m)
Condition I	40	2.5
Condition II	40	3.5
Condition III	40	4.5
Condition IV	37	2.5
Condition V	43	2.5

Optimizations were accomplished though using MATLAB. Taking the digging condition I (digging distance set to 2.5 m and the slope angle set to 40°) as an example, the Pareto results are shown in Figure 12a, and the corresponding distribution of the variables is shown in Figure 12b.

(**a**) Pareto front

(**b**) Pareto results
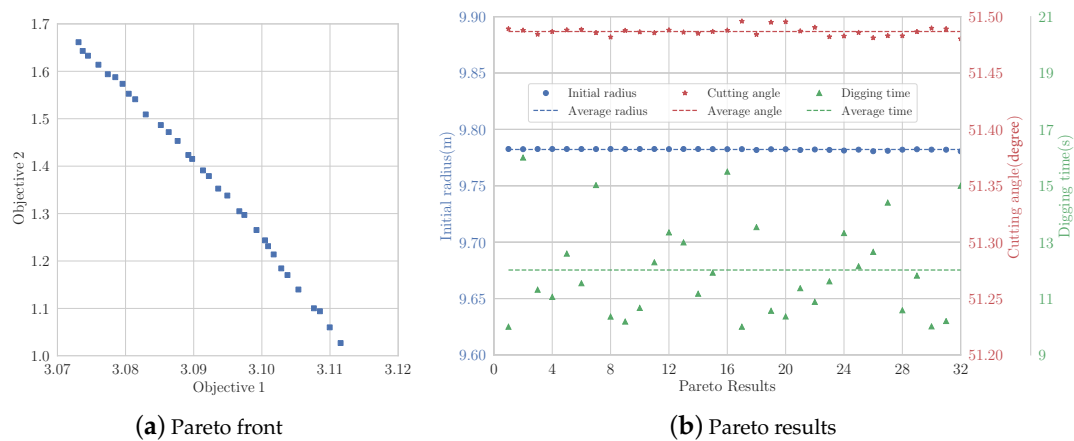
Figure 12. First phase optimization results for Condition I.

As shown in Figure 12b, the design variables of the initial polar diameter and soil cutting angle converged to a concentrated interval with the individual values slightly fluctuating around the average value. However, the design variable of digging time was distributed around the average value discretely. Hence, the digging time was taken as the indicator for deciding the optimal combination of the design variables based on the Pareto results. Similarly, the first phase optimizations were applied to the other four digging conditions with the optimal results listed in Table 6.

Table 6. First phase optimization results for all five digging conditions.

Digging Condition	ρ_0 (m)	δ_d (degree)	t_{dig} (s)	$F_{hoist_{max}}$ (kN)	$F_{crowd_{max}}$ (kN)	$P_{hoist_{max}}$ (kW)	$P_{crowd_{max}}$ (kW)	Fullness	E/M (J/kg)
I	9.78	51.5	10.02	3487.42	860.08	3218.10	265.08	0.9598	271.2458
II	9.96	48.5	10.04	3497.75	882.96	3524.60	351.20	0.9603	284.1154
III	10.02	45.1	10.11	3489.99	915.91	3683.09	452.16	0.9481	296.8358
IV	9.95	49.8	10.07	3492.24	913.31	3311.64	327.52	1.0126	268.8554
V	9.52	51.1	10.04	3498.95	749.14	3180.14	237.15	0.8995	274.8638

Comparing the data listed in Tables 2 and 6, the digging parameters applied in the first phase optimization were set the same as the real tested area in the Anjialing mining site, and after the first phase optimization, the digging time of all five digging conditions decreased dramatically from the minimum of 15 s to an average of about 10 s. Besides, different digging conditions slightly affected the optimization result of bucket fullness, which stably stayed above 0.9. The data listed in Table 6 indicated that the different digging conditions had a different influence on the optimization results. With the same digging distance, when the value of the slope angle increased, the optimal initial polar diameter became shorter, while the soil cutting angle almost remained the same. However, the optimal cutting angle kept decreasing while the initial polar diameter barely changed when the digging distance increased with a constant value of the slope angle. Additionally, the unit energy consumption per payload increased with the digging distance, as well as the slope angle. Hence, in general, under the condition that the materials had similar properties and a regular particle size distribution, the digging distance influenced the digging operation more significantly than the slope angle.

5.3.2. Material Piled up with a Curved Surface

Even in the ideal digging conditions, it was difficult to guarantee that every piled-up material profile could be simplified as a flat surface using a value of the slope angle for the description. In order to keep in line with the same diggability of the material in the Anjialing mining site, the same values of the digging parameters were applied. Hence, based on a slope angle of 40°, four curved profiles were established

representing four typical concave-convex conditions. For each curved profile, three digging distance were applied for digging trajectory optimization, as shown in Figure 13.

(**a**) d_m = 2.5 m, Curve 1   (**b**) d_m = 3.5 m, Curve 1   (**c**) d_m = 4.5 m, Curve 1

(**d**) d_m = 2.5 m, Curve 2   (**e**) d_m = 3.5 m, Curve 2   (**f**) d_m = 4.5 m, Curve 2

(**g**) d_m = 2.5 m, Curve 3   (**h**) d_m = 3.5 m, Curve 3   (**i**) d_m = 4.5 m, Curve 3

(**j**) d_m = 2.5 m, Curve 4   (**k**) d_m = 3.5 m, Curve 4   (**l**) d_m = 4.5 m, Curve 4
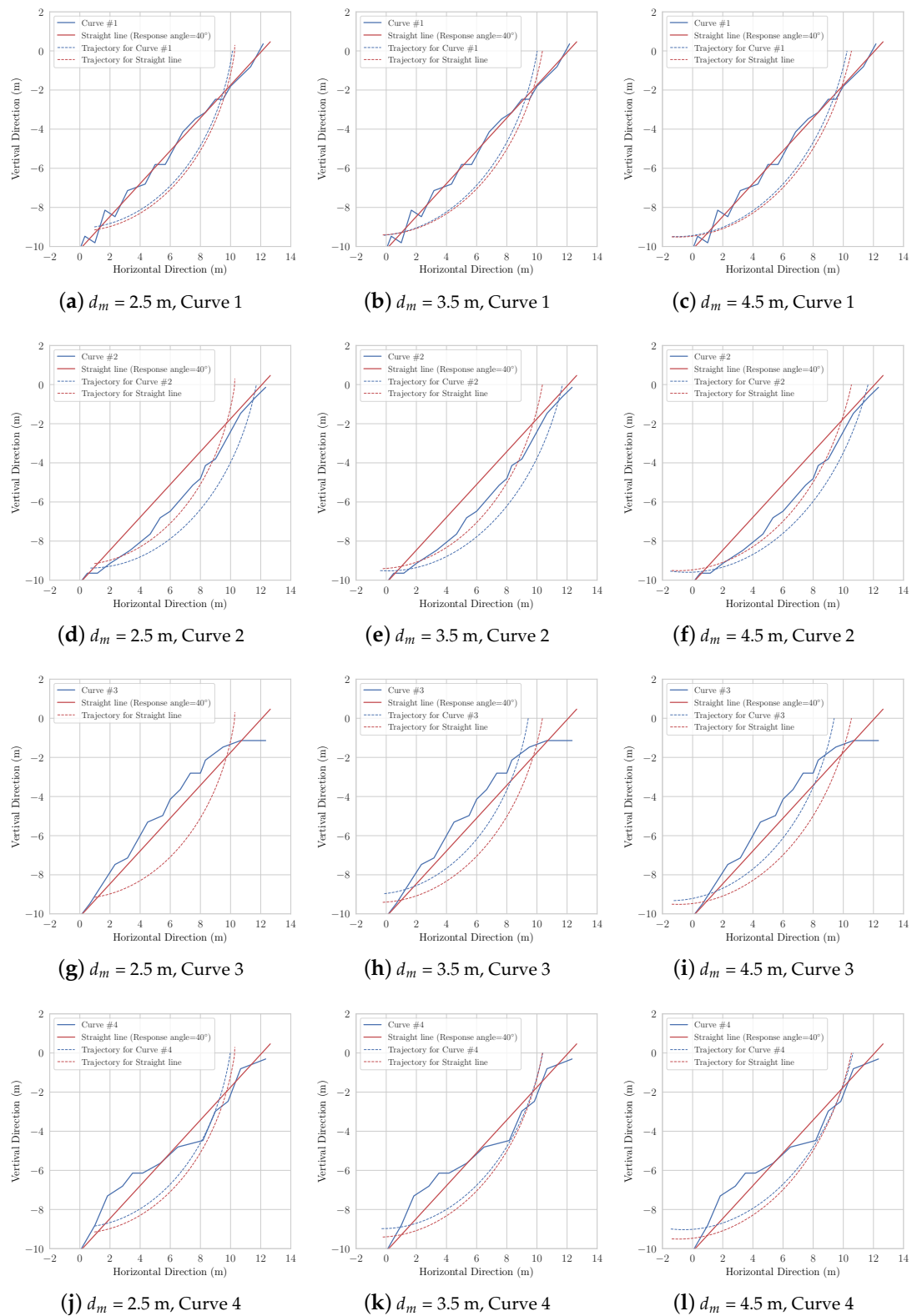
Figure 13. Digging trajectories for Curves 1–4: first phase optimization.

It can be seen from Figure 13 that the profile of piled-up material dramatically influenced the optimization results. In other words, the optimization method established in this research could adapt to various digging conditions. The digging performance comparisons between the optimal digging trajectories for different piled-up material profiles are listed in Table 7.

Table 7. Digging performance comparison between digging trajectories: first phase optimization.

Material Pile	ρ_0 (m)	δ_d (degree)	t_{dig} (s)	$P_{hoist_{max}}$ (kW)	$P_{crowd_{max}}$ (kW)	Fullness	E/M (J/kg)
Digging Distance d_m = 2.5 m							
Curve 1	9.64	51.5	10.00	3146.10	235.08	0.8427	277.0546
Curve 2	9.91	47.5	10.01	3434.60	338.74	0.9442	293.3497
Curve 3	–	–	–	–	–	–	–
Curve 4	9.50	51.5	10.00	2426.30	367.74	0.8047	266.2236
Straight Line	9.78	51.5	10.02	3218.10	265.08	0.9598	271.2458
Digging Distance d_m = 3.5 m							
Curve 1	10.02	49.8	10.02	3419.90	287.18	0.8461	292.0918
Curve 2	9.98	44.6	10.00	3922.00	390.78	0.8598	312.9045
Curve 3	9.58	50.2	10.00	3480.90	340.32	0.8514	286.4528
Curve 4	9.53	46.8	10.01	2813.40	528.62	0.8630	278.2105
Straight Line	9.96	48.5	10.04	3524.60	351.20	0.9603	284.1154
Digging Distance d_m = 4.5 m							
Curve 1	10.00	45.9	10.03	3695.70	398.55	0.8298	308.2182
Curve 2	10.04	42.0	10.00	3674.60	426.56	0.7150	348.2000
Curve 3	9.87	48.1	10.10	3756.90	426.98	0.8459	302.7920
Curve 4	9.50	42.9	10.04	3007.60	673.70	0.8524	291.8544
Straight Line	10.02	45.1	10.11	3683.09	452.16	0.9481	296.8358

Combining the data listed in Table 7 and the information shown in Figure 13, the relationship between the piled-up material profile and the optimal digging trajectory could be summarized into the following aspects: For Curve 2 and Curve 3, the curved profile entirely stayed above or beneath the 40° slope line, and the corresponding digging trajectories moved forward and backward accordingly. It should be noted that, for Curve 3, there did not exist an optimal digging trajectory for the case with the digging distance of 2.5 m, which indicated that there was no optimal result fitting the constraints if the cable shovel stayed too close to the material pile. Similarly, the digging trajectories corresponding to Curve 1 appeared close to those optimized for the 40° slope line because the curve itself just fluctuated slightly around the line. For Curve 4, however, the optimization made the digging trajectory fill the bucket during the early period of excavation, which matched with the character of this curve and reduced the energy consumption per payload.

The results indicated that the first phase optimization could adapt to different digging conditions. Although the digging conditions set in this research for digging trajectory optimization could not cover all kinds of operational demands, the optimal results could prove the validity of the optimization to some extent.

5.4. Second Phase Optimization

Based on the results of the first phase optimization, the second phase optimization was carried out to enhance the executability of the excavation process while improving the digging performance.

Taking the digging for Condition I as an example, the comparison between the results of the first and second phase optimization are shown in Figure 14.

(**a**) Digging trajectory　　　　　(**b**) Digging radius　　　　　(**c**) Hoist velocity

(**d**) Crowd velocity　　　　　(**e**) Crowd power　　　　　(**f**) Hoist power
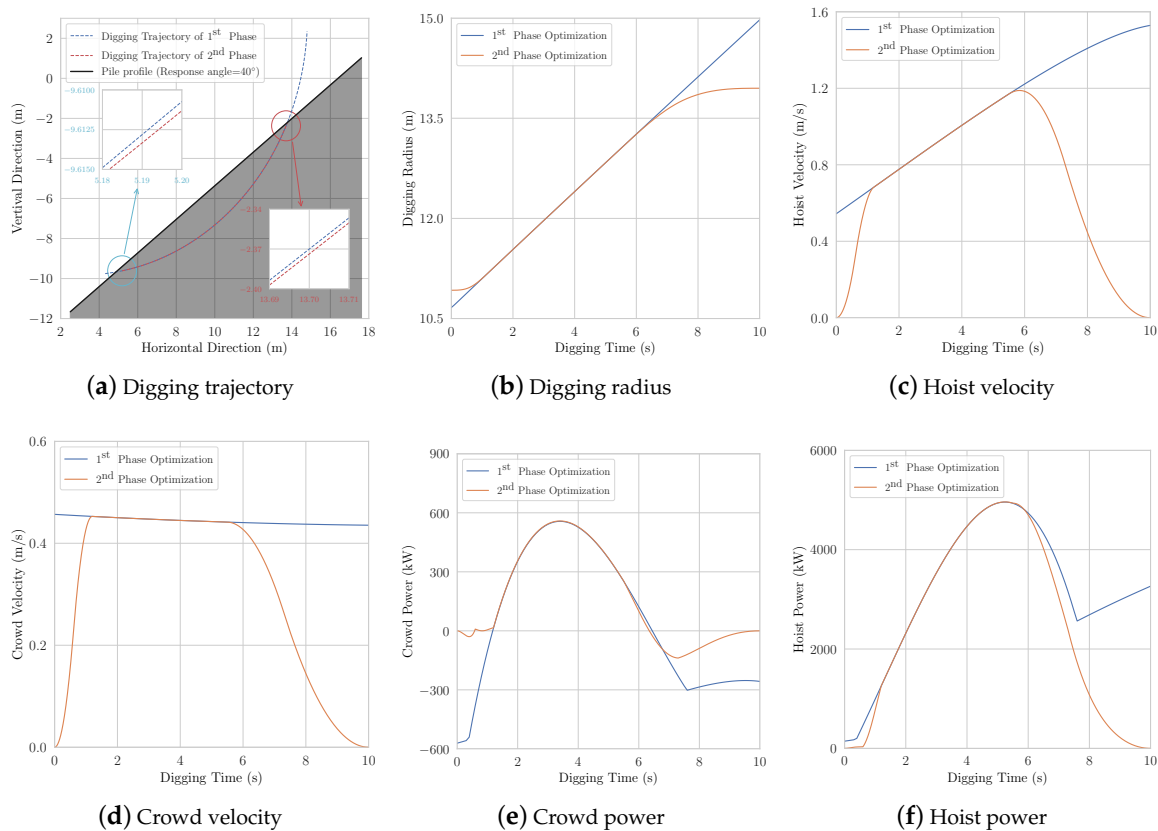
Figure 14. Digging performance comparison between two phases of optimization: an example.

As can be seen from Figure 14a, the total length of the digging trajectory reduced significantly after the second phase optimization, while the shape of the trajectory mostly retained the result of the first phase optimization with a slight difference that appeared at both ends of the trajectory. It is also clearly shown in Figure 14a that after the second phase of optimization, the digging process stopped right after the shovel bucket totally moved above the material slope. As the cable shovels are usually switched to swing cycle after the digging cycle, it might help prevent the shovel bucket from hitting the bench face for the operators to hoist the bucket much higher than the material pile, but that is not necessary for robotic excavations. Hence, the trajectory from the second phase optimization was more reasonable than the result of the first phase optimization. Besides, the constraints applied in the second phase of optimization ensured the smooth change of kinematic and performance parameters, which made the digging process more practical by reducing the impact force during the digging process. As shown in Figure 14b–f, either the speed or the power consumption of the driving system started and ended with the value of zero. The results of all digging conditions are listed in Table 8.

Table 8. The results of the second phase optimization.

Digging Condition	t_1 (s)	t_2 (s)	t_3 (s)	t_4 (s)	$F_{hoist_{max}}$ (kN)	$F_{crowd_{max}}$ (kN)	$P_{hoist_{max}}$ (kW)	$P_{crowd_{max}}$ (kW)	*Fullness*	*E/M* (J/kg)
I	0.4	1.2	6.5	9.6	3486.20	863.51	3217.63	266.09	0.9579	237.0699
II	1.0	2.4	6.9	9.6	3499.11	885.83	3527.50	352.32	0.9603	244.5252
III	2.1	3.7	8.1	9.5	3492.75	919.28	3642.87	453.80	0.9481	252.7828
IV	0.4	1.2	5.7	9.6	3489.84	918.27	3315.66	329.30	1.0126	226.4975
V	0.4	2.3	8.1	9.5	3499.98	751.05	3182.23	237.74	0.8995	250.0330

Combining the data listed in Tables 6 and 8, the comparison between the digging performance of the first and second phase optimization results is shown in Figure 15.

(**a**) Comparison of maximum hoist power

(**b**) Comparison of maximum crowd power

(**c**) Comparison of bucket fullness

(**d**) Comparison of unit energy consumption
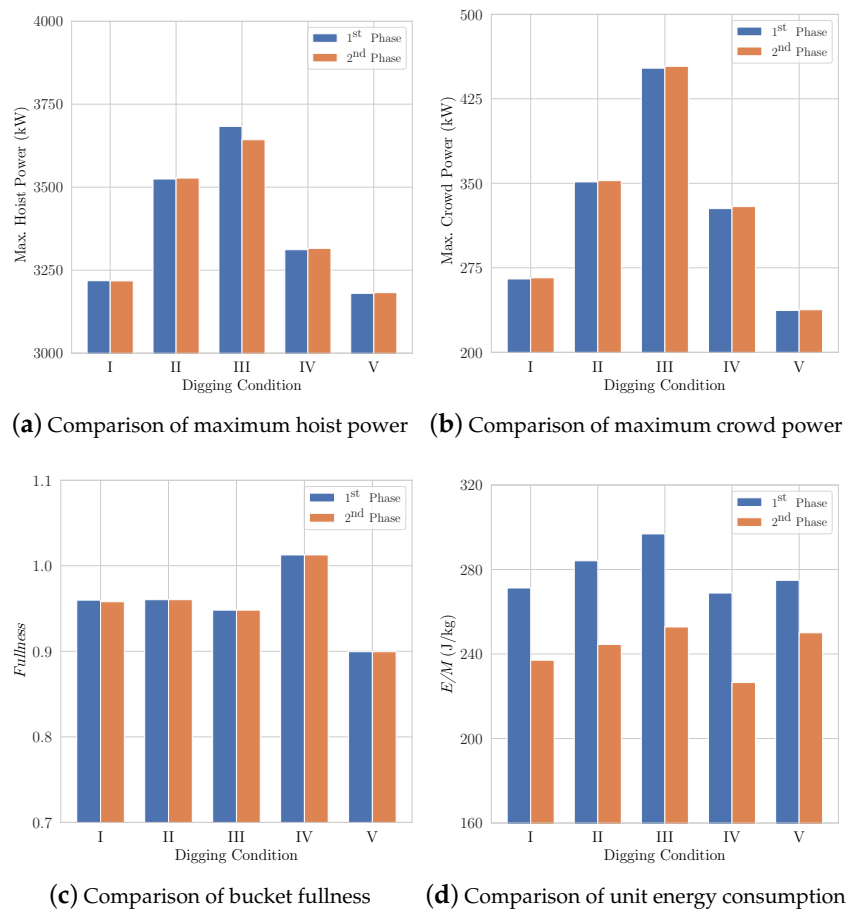
Figure 15. Digging performance comparison between two phases of optimization.

As shown in Figure 15, the unit energy consumption per payload was the only parameter of digging performance that significantly changed after the second phase of optimization. To be more specific, the reduction of all five digging conditions was on average 13.28%. In other words, the second phase optimization mainly retained the advantage of the results of the first phase optimization with the energy consumption further decreased while making the digging trajectory more practical.

6. Conclusions

A kind of multi-objective two-phase optimization method was established for robotic excavation of cable shovels in this research. The cable shovel with a nominal dipper capacity of about 55 m^3 (WK-55) was applied for the validation of the optimization method under various digging conditions with different forms of pile-up material and digging distance. Field tests were applied in the Anjialing mining site for the measurement of the digging performance of the cable shovel and the rational selection of the digging parameters. It could be concluded from the optimization process that different digging conditions corresponded to different optimal digging trajectories. However, if the shovel stayed too close to the material slope, there might not exist an optimal result for the digging trajectory. Therefore, the shovels should stay at a reasonable distance toward the material slope for an optimal digging process. The two-phase optimization took theoretical advantage of the digging trajectory with a constant value of soil cutting angle and overcame its weakness in executability. Under the same material condition of the Anjialing mining site, the optimization results indicated

that the average digging time decreased from 20 s driven by operators to 10 s after the first phase optimization. The unit energy consumption reduced by 13.28% after the second phase optimization. The optimization experiments under different digging conditions and the corresponding results proved that the two-phase optimization method established in this research was an adaptive and effective method for optimal digging trajectory planning.

References

1. Darling, P. *SME Mining Engineering Handbook*, 3rd ed.; Society for Mining, Metallurgy, and Exploration: Englewood, CO, USA, 2011.

2. BabaeiKhorzoughi, M.; Hall, R. A study of digging productivity of an electric rope shovel for different operators. *Minerals* **2016**, *6*, 2.

3. Blackwell, G.H. Remote and Semi-Automated Operation of an Electric Cable Shovel Author. 2013. Available online: http://www.iaarc.org/publications/fulltext/isarc2013Paper419.pdf (accessed on 15 June 2020).

4. Awuah-Offei, K.; Frimpong, S. Cable shovel digging optimization for energy efficiency. *Mech. Mach. Theory* **2007**, *42*, 995–1006. [CrossRef]

5. Dunbabin, M.; Corke, P. Autonomous excavation using a rope shovel. *J. Field Robot.* **2006**, *23*, 379–394. [CrossRef]

6. Wei, B.; Gao, F. Digging trajectory optimization for a new excavating mechanism of electric mining shovel. In Proceedings of the ASME 2012 International Design Engineering Technical Conferences and Computers and Information in Engineering Conference, Chicago, IL, USA, 12–15 August 2012.

7. Wang, X.; Sun, W.; Li, E.; Song, X. Energy-minimum optimization of the intelligent excavating process for large cable shovel through trajectory planning. *Struct. Multidiscip. Optim.* **2018**, *58*, 2219–2237. [CrossRef]

8. Xu, G.; Ding, H.; Feng, Z. Optimal Design of Hydraulic Excavator Shovel Attachment Based on Multiobjective Evolutionary Algorithm. *IEEE Trans. Mechatronics* **2019**, *24*, 808–819. [CrossRef]

9. Jang, G.; Cho, S.-B. Optimal Trajectory Path Generation for Jointed Structure of Excavator using Genetic Algorithm. In Proceedings of the 2019 IEEE Congress on Evolutionary Computation (CEC), Wellington, New Zealand, 10–13 June 2019.

10. Yu, X.; Pang, X.; Zou, Z.; Zhang, G.; Hu, Y.; Dong, J.; Song, H. Lightweight and High-Strength Design of an Excavator Bucket under Uncertain Loading. *Math. Probl. Eng.* **2019**. [CrossRef]

11. Feng, H.; Yin, C.-B.; Weng, W.-W.; Ma, W.; Zhou, J.-J.; Jia, W.-H.; Zhang, Z.-L. Robotic excavator trajectory control using an improved GA based PID controller. *Mech. Syst. Signal Process.* **2018**, *105*, 153–168. [CrossRef]

12. Li, X.; Wang, G.; Miao, S.; Li, X. Optimal design of a hydraulic excavator working device based on parallel particle swarm optimization. *J. Braz. Soc. Mech. Sci. Eng.* **2017**, *39*, 3793–3805. [CrossRef]

13. Kim, J.-W.; Jung, S.; Kim, J.; Kim, J.; Seo, T. Optimal design of the front linkage of a hydraulic excavator for multi-objective function. *J. Mech. Sci. Technol.* **2014**, *28*, 3103–3111. [CrossRef]

14. Barakat, N.; Sharma, D. Evolutionary multi-objective optimization for bulldozer and its blade in soil cutting. *Int. J. Manag. Sci. Eng.* **2019**, *14*, 102–112. [CrossRef]

15. Masih-Tehrani, M.; Ebrahimi-Nejad, S. Hybrid Genetic Algorithm and Linear Programming for Bulldozer Emissions and Fuel-Consumption Management Using Continuously Variable Transmission. *J. Constr. Eng. Manag.* **2018**, *144*, 7. [CrossRef]

16. Zhang, Z.; He, B. Comprehensive optimum and adaptable design methodology for the working mechanism of a wheel loader. *Int. J. Adv. Manuf. Technol.* **2018**, *94*, 3085–3095. [CrossRef]

17. Cao, B.-W.; Liu, X.-H.; Chen, W.; Zhang, Y.; Li, A.-M. Depth Optimization Analysis of Articulated Steering Hinge Position Based on Genetic Algorithm. *Algorithms* **2019**, *12*, 3. [CrossRef]

18. Zelenin, A.; Balovnev, V.; Kerov, I. *Machines for Moving the Earth: Fundamentals of the Theory of Soil Loosening, Modeling of Working Processes and Forecasting Machine Parameters*; United States Department of Agriculture, and the National Science Foundation: Washington, DC, USA, 1985.